



Title	Observation of Synchronization Between Instabilities of the Sporadic E Layer and Geomagnetic Field Line Connected F Region Medium-Scale Travelling Ionospheric Disturbances
Authors	Mitsumu K. Ejiri, Takuji Nakamura, Takuo T. Tsuda, Takanori Nishiyama, Makoto Abo, Chiao-Yao She, Michi Nishioka, Akinori Saito, Toru Takahashi, Katsuhiko Tsuno, Takuya D. Kawahara, Takayo Ogawa, Satoshi Wada
Citation	JGR Space Physics, 124, 4627-4638, 2019
Issue Date	2019-6-18
Type	Journal Article
URL	https://doi.org/10.1029/2018JA026242
Right	
Textversion	publisher

JGR Space Physics

RESEARCH ARTICLE

10.1029/2018JA026242

Key Points:

- The irregularities of the E_s layer and the MSTIDs were observed simultaneously by a Ca^+ lidar, an ionosonde, and a GNSS receiver network
- The simultaneous observation clearly revealed how the E_s layer and the F region ionosphere are coupled
- This is the first synchronous observation of the coupling between the density irregularities of the E_s layer and the MSTIDs in the F region

Correspondence to:

M. K. Ejiri,
ejiri.mitsumu@nipr.ac.jp

Citation:

Ejiri, M. K., Nakamura, T., Tsuda, T. T., Nishiyama, T., Abo, M., She, C.-Y., et al. (2019). Observation of synchronization between instabilities of the sporadic E layer and geomagnetic field line connected F region medium-scale traveling ionospheric disturbances. *Journal of Geophysical Research: Space Physics*, 124, 4627–4638. <https://doi.org/10.1029/2018JA026242>

Received 21 NOV 2018

Accepted 8 MAY 2019

Accepted article online 20 MAY 2019

Published online 18 JUN 2019

Observation of Synchronization Between Instabilities of the Sporadic E Layer and Geomagnetic Field Line Connected F Region Medium-Scale Traveling Ionospheric Disturbances

Mitsumu K. Ejiri^{1,2}, Takuji Nakamura^{1,2}, Takuo T. Tsuda³, Takanori Nishiyama^{1,2}, Makoto Abo⁴, Chiao-Yao She⁵, Michi Nishioka⁶, Akinori Saito⁷, Toru Takahashi^{1,8}, Katsuhiko Tsuno⁹, Takuya D. Kawahara¹⁰, Takayo Ogawa⁹, and Satoshi Wada⁹

¹National Institute of Polar Research, Tachikawa, Japan, ²Department of Polar Science, SOKENDAI, The Graduate University for Advanced Studies, Tachikawa, Japan, ³Department of Computer and Network Engineering, University of Electro-Communications, Chofu, Japan, ⁴Department of Electrical Engineering and Computer Science, Tokyo Metropolitan University, Hino-shi, Japan, ⁵Department of Physics, Colorado State University, Fort Collins, CO, USA, ⁶National Institute of Information and Communications Technology, Koganei, Japan, ⁷Graduate School of Science, Kyoto University, Kyoto, Japan, ⁸Now at Department of Physics, University of Oslo, Oslo, Norway, ⁹RIKEN, RAP, Wako, Japan, ¹⁰Faculty of Engineering, Shinshu University, Nagano, Japan

Abstract A frequency-tunable resonance scattering lidar with high temporal/vertical resolutions (1 min/15 m) observed sporadic calcium ion (Ca^+) layers at ~100 km over Tachikawa (geographical/geomagnetic latitude: 35.7°N/27.1°N), Japan, on 21–22 August 2014. Simultaneously, sporadic E (E_s) parameters and medium-scale traveling ionospheric disturbances (MSTIDs) were observed by an ionosonde and Global Navigation Satellite System receiver network, GEONET, respectively. The maximum densities of the Ca^+ and electrons in the E_s layer had a strong positive correlation. As observation started ~23:30 LT, the Ca^+ layer and the associated E_s layer descended at ~2.8 km/hr with density irregularities including Kelvin-Helmholtz billow-like structures suggesting the presence of background neutral wind shear and instability. And the total electron content variations showed large amplitude associated with the MSTIDs at an altitude of 300 km in synchronization with the Ca^+ column abundance surges at 100 km over Tachikawa; in their respective E and F region locations connected by geomagnetic field line these irregularities are found to vary in phase. At ~02:00 LT, the Ca^+ layer stopped descending at ~100 km due to larger ion-neutral collision frequency in the lower altitudes and resided there quietly until sunrise; both Ca^+ column abundance enhancements and the large total electron content variation disappeared as the descent of the Ca^+ layer stopped, implicating that the MSTID structure cannot be sustained without the density irregularities of the E_s layer. This is the first synchronous observation of the coupling between the E_s density irregularities and the MSTIDs in the F region along a common magnetic flux tube.

Plain Language Summary The irregular structures of the sporadic E (E_s) layer appearing in altitudes of 90–130 km were observed by a calcium ion (Ca^+) resonance scattering lidar and an ionosonde. Simultaneously, medium-scale traveling ionospheric disturbances (MSTIDs) in the F region (150- to 500-km altitude) were observed by the Global Navigation Satellite System receiver array in Japan. Though the electron column abundance variation in the E_s irregularities is more than an order of magnitude smaller than that in the MSTIDs, we observed that the MSTIDs decayed with the disappearance of the irregular structure in the E_s layer. This observation clearly revealed for the first time that the plasma density irregularities in the E region were coupled to those in the F region by the geomagnetic field line as theory predicted.

1. Introduction

The sporadic E (E_s) layer is a thin plasma layer in the E region ionosphere. It frequently appears at midlatitudes in the summertime (e.g., Haldoupis, 2012; Whitehead, 1989). It is widely believed that the formation of the E_s layer in the midlatitude is attributed to the vertical shear of the neutral wind in the lower thermosphere (Whitehead, 1961). Around the E_s layer altitudes, very high frequency radars have observed meter-scale field-aligned irregularities and have found quasiperiodic (QP) echoes appearing intermittently in periods of 5–20 min (e.g., Yamamoto et al., 1991, 1992, 1994). Employing the Middle and Upper

Atmosphere Radar (MU radar) observations at Shigaraki, Japan, Yamamoto et al. (1994) found monochromatic wave structured QP echoes with horizontal wavelengths of 5–15 km, propagating toward the SSW direction with wavefronts aligned along the northwest-southeast (NW-SE) direction. Through simultaneous observations at Shigaraki with the MU radar and an ionosonde, Ogawa et al. (2002) found that the QP echoes appear in the MU radar echo with the difference between the critical E_s frequency, f_oE_s , and the blanketing frequency, f_bE_s , exceeding 1 MHz, implicating spatial inhomogeneity in the E_s layer. The sounding rocket measurement magnesium ion imager has provided clear horizontal patchy structures of magnesium ion (Mg^+) density distribution in the E_s layer (Kurihara et al., 2010).

In the mesosphere and lower thermosphere (MLT) region, the vertical structure of the E_s layer has been profiled by measuring the ion and electron densities, respectively, with a resonance scattering lidar and an incoherent scatter (IS) radar. Here, several metallic atom and ion layers exist; historically, these metallic atoms and ions have been observed by rocketborne mass spectrometers (e.g., Istomin, 1963). In recent years, the availability of resonance scattering lidars made it possible to observe metallic atom layers (e.g., Na, K, Ca, and Fe) in the MLT region regularly and in high vertical resolution. However, since the resonance transition wavelength of many metal ions is shorter than 300 nm, they cannot be measured from ground due to strong absorption of stratospheric ozone. Calcium (Ca) appears to be the only upper mesospheric metal with a strong ion resonance transition at a wavelength longer than 300 nm (Ca^+ at 393.37 nm). The first Ca^+ lidar observation is performed at Haute-Provence, France (43.9°N, 5.7°E), by Granier et al. (1985). Thereafter, typical parameters of the Ca^+ layer, such as seasonal variation in Ca^+ density and the relationship between sporadic Ca (atom) and Ca^+ (ion) layers, were investigated at K uhlungsborn, Germany (54.1°N, 12.8°E; Gerding et al., 2000, 2001). Taking the advantage of IS radar's capability to vertically resolve electron density, recent lidar measurements at the Arecibo Observatory (18.4°N, 66.8°W) showed that Ca^+ layers are often correlated with the electron layers (Raizada et al., 2011, 2012; Tepley et al., 2003). The observed good positive correlation between the Ca^+ and electron densities indicated a one-to-one relationship, making the Ca^+ density a reliable proxy of the E_s layer. In addition, Raizada et al. (2012) showed that the averages of Ca^+ density to electron density ratio in summer were more than twice the values in winter in the altitude range of 89–100 km, and the average ratios above 101 km were 0.3–0.5% in both summer and winter.

In the ionospheric F region at midlatitudes, nighttime medium-scale traveling ionospheric disturbances (MSTIDs) have been studied intensively using various observational techniques. The frontal structures of the MSTIDs have been identified by all-sky images in the 630-nm airglow (e.g., Miller et al., 1997; Shiokawa et al., 2003) and by the two-dimensional maps of the total electron content (TEC) detected by the Global Navigation Satellite System (GNSS) receiver array (e.g., Saito et al., 1998, 2001). The observed nighttime MSTIDs in the Northern Hemisphere were elongated along the NW-SE direction and propagated the SW direction with horizontal wavelengths of 100–300 km and horizontal phase velocities of 50–250 m/s.

Indirect measurement of the E_s layer using QP echoes from the field-aligned irregularities of the E region was carried out with very high frequency radars to investigate the coupling process between the E_s layer and the MSTIDs (Saito et al., 2007; Zhou et al., 2018), and a close relationship was observed between the QP echoes and the MSTIDs. Otsuka et al. (2008) conducted a statistical study using TEC and the E_s parameters obtained by an ionosonde and found that the MSTID activity is closely correlated with the plasma frequency parameters f_oE_s and $\Delta f (=f_oE_s - f_bE_s)$. Although this relation suggests that the MSTIDs in the F region are closely related with the E_s layer and its spatial inhomogeneity, it is difficult to compare the MSTIDs and E_s layer events directly because the field of view (FOV) of ionosondes is much wider than the horizontal scale of the E_s layer, and ionosondes cannot observe the vertical structures of the E_s layer. Consequently, the coupling between the plasma density structures of the E_s layer and the MSTIDs has not yet been directly observed.

The Perkins instability (Perkins, 1973) was proposed as the generation mechanism of plasma structures in the F region. The growth rate was, however, too low to explain the observed amplitude of the MSTIDs. To increase the growth rate of the Perkins instability, a coupling process between the E_s layer instability and the Perkins instability was proposed. With both instabilities included, a larger growth rate was demonstrated by Cosgrove and Tsunoda (2004) and Tsunoda (2006). Later observations (Otsuka et al., 2007; Saito et al., 2007) showed evidence of simultaneous occurrence of MSTIDs and QP echoes on a common magnetic flux tube. Such a connection and the growth of the MSTIDs have been reproduced by three-dimensional

numerical studies that include the E - F coupling process (Swartz et al., 2009; Yokoyama et al., 2009; Yokoyama & Hysell, 2010). Despite the progress in numerical model studies, it is difficult to measure electron density variations simultaneously in the ionospheric E region and F region connected by the geomagnetic field lines directly. Simultaneous observation of E region and F region at one well equipped site, such as Arecibo, cannot reliably reveal this connection. The main purpose of this paper is thus to report the simultaneous observation of Ca^+ density in the E_s layer at one site (Tachikawa) and GPS TEC maps of the F region over a larger area, from which we can reveal the E - F coupling along a common magnetic flux tube.

A new resonance scattering lidar was installed at the National Institute of Polar Research (NIPR) in Tachikawa (35.7°N, 139.4°E), Japan, as part of an Antarctic research project. Using this ground-based resonance scattering lidar, we measured Ca^+ density profiles in the MLT region on 21–22 August 2014 over Tachikawa, a midlatitude site. On the same night, the E_s layer was observed with an ionosonde at the National Institute of Information and Communications Technology (NICT) in Kokubunji (35.7°N, 139.5°E), Japan. The distance between the lidar and the ionosonde is only 7.5 km. Further, MSTIDs were observed using the dense GNSS receiver network, GEONET, in Japan. We compared these data and clearly revealed relationships between the Ca^+ density variations, E_s layer irregularities, and the MSTIDs for the first time.

2. Observations

2.1. Frequency-Tunable Resonance Scattering Lidar

In the new resonance scattering lidar system with tunable laser wavelengths deployed at the NIPR, the lidar transmitter has two units. One is an injection-seeded, pulsed alexandrite ring laser specially designed by Light Age and Megaopto for fundamental wavelengths of 768–788 nm, and the other is a second-harmonic generation unit with two nonlinear crystals, Beta Barium Borate, producing wavelengths of 384–394 nm. The wavelengths of a seed laser, Toptica DL pro 780, are tuned to the resonance wavelengths of atoms or ions by proportional integral derivative control with a HighFinesse WSU-10 wavelength meter that is well calibrated using a wavelength-stabilized He-Ne laser. The resonance scattering lidar has capabilities to measure density profiles of minor constituents such as atomic iron (Fe at 386 nm), atomic potassium (K at 770 nm), calcium ion (Ca^+ at 393 nm), and auroral excited nitrogen ion (N_2^+ at 390 and 391 nm). Also, temperature profiles in the MLT region can be measured based on the resonance scattering spectrum of Fe or K. The reception telescope was a Nasmyth-Cassegrain $f/8$ telescope, manufactured by Kiyohara Optics Inc., with a 0.8-m diameter primary mirror. The photons were detected by a Hamamatsu R9880U-210 ultra bi-alkali photomultiplier tube attached to the back of the telescope. The photon counts were recorded using a Licel transient recorder, PR10-160-P.

The resonance scattering lidar at the NIPR was tuned to 393 nm, and the Ca^+ density profiles were measured from 23:13 LT on 21 August 2014 to 04:28 LT on 22 August 2014. The average laser power of the Ca^+ resonance wavelength was 80 mW with a repetition rate of 24.3 Hz. The range resolution was 165 m (15-m sampling data smoothed by 165-m running average), and the temporal resolution was 1 min with an integration time of ~ 50 s for 1,250 pulses. The background noise was reduced using a band-pass filter having a center wavelength of 389.7 nm and a full width at half maximum of 11.5 nm. The Ca^+ densities were derived using equation (5.38) from the textbook Laser Remote Sensing (cf. Chu & Papen, 2005, p. 208). The Rayleigh scattering cross section was calculated from that of air molecules at 532 nm given in She (2001). The average count in the 200- to 230-km altitude range of each profile was regarded as the background count for that profile. The background-subtracted counts were normalized by the Rayleigh signal at 35-km altitude to yield Ca^+ densities. Since the deviation from the average background count could be larger than the average background count, the background-subtracted counts may have occasionally negative values; these data with a signal-to-noise ratio less than 2.0 (corresponding to an error larger than 50%) were filtered out and removed in this study.

2.2. Ionosonde

Kokubunji (35.7°N, 139.5°E), 7.5 km away from Tachikawa, is one of the four NICT stations with routine ionosonde operation. Ionograms are obtained in every 15 min with a 15-s sweep time from 1 to 30 MHz. For example, an ionogram of 23:00 LT is obtained by a sweep from 23:00:00 LT to 23:00:15 LT. E_s layer

parameters, the critical (f_oE_s) and blanketing (f_bE_s) frequencies, were determined from the ionogram. f_oE_s and f_bE_s correspond to the maximum and minimum electron densities, respectively, in the E_s layer within the FOV of the ionosonde. A large frequency difference $\Delta f (= f_oE_s - f_bE_s)$ indicates a large difference in plasma density in the E_s layer within the FOV of the ionosonde. The ionograms obtained from 23:00 LT on 21 August to 04:00 LT on 22 August 2014 showed the presence of E_s layers around 100-km altitude.

2.3. GNSS Receiver Network

The GPS TECs between the GEONET receivers and GPS satellites can be derived from the measured phases of the two carrier waves with different frequencies (Saito et al., 1998). The GEONET is the dense GNSS receiver network that consists of more than 1,000 GNSS receivers all over Japan, installed and operated by the Geographical Survey Institute of Japan. The GPS TECs were derived every 30 s. Data from GPS satellites with elevation angles higher than 35° were used in this analysis. To provide for the perturbation component of the GPS TECs (detrended GPS TECs), the large-scale trend of the TEC for each transmitter-receiver pair, determined from the 1-hr running average, was subtracted. The detrended GPS TECs were converted into vertical values by assuming that all the contributions to the slant TECs were from a virtual thin layer at an altitude of 300 km. In this study, the vertical values are used as the GPS TECs. The temporal variation of the GPS TECs is associated with the MSTIDs. On the night of 21 August 2014, the typical values of the background GPS TECs over Japan were $10\text{--}20 \times 10^{16} \text{ m}^{-2}$, and the amplitude of temporal variation of the GPS TECs was $\sim 2 \times 10^{16} \text{ m}^{-2}$.

3. Results and Discussion

3.1. Sporadic Ca^+ Layer

The temporal variations of Ca^+ density profiles in the height range of 80–130 km from 23:13 LT on 21 August 2014 to 04:28 LT on 22 August 2014 are shown in Figure 1a. Three thin and high-density layers (hereinafter referred to as sporadic Ca^+ [Ca^+_s] layer) were observed. The Ca^+_s layer with the highest density was observed at 97–110 km for the whole night (hereinafter referred to as the main Ca^+_s layer). The other two layers were observed only for a few hours. One layer with relatively low density was seen between ~ 88 - and 97-km altitude from 23:45 LT to 02:00 LT, and another layer was seen between 115 and 121 km from 03:10 to 04:15 LT with a density comparable to that of the main Ca^+_s layer observed at the same time.

The main Ca^+_s layer descended from 107 km at 23:30 LT to ~ 100 km at 02:00 LT with large changes and irregularities in density and layer width and then stayed at ~ 100 km without such changes until sunrise. The density irregularities of the Ca^+_s layer seen repeatedly before $\sim 02:00$ LT had various fine structures. As examples, two of them were enlarged for clarity. Figure 1b displays the height range of 101–107 km in a time range of 00:25–00:45 LT. Two clumps with high density are seen from 00:30 LT to 00:37 LT and from 00:43 LT to 00:45 LT. The fine structure in the later clump was unclear, while the former clump showed a small-scale wave-like structure with a wave period of ~ 2 min and a peak-to-peak height variation of ~ 2 km. The temporal variation of the density was rapid and large and varied by more than 1 order of magnitude for a few minutes. The irregular structure was probably caused not only by neutral atmospheric dynamics but also by plasma irregularities such as the E - F coupling process (Hysell et al., 2018). In section 3.3, we will present the results of comparison of the density irregularity of the Ca^+_s layer with the ionospheric disturbances in the F region observed as GPS TEC variations. The other irregular structure with a small change of density and a large change of layer width is displayed in Figure 1c in the height range of 100–105 km and a time range of 01:00–01:20 LT. A rolling structure, similar to a Kelvin-Helmholtz (K-H) billow, is clearly seen between 01:05 LT and 01:12 LT. As ion-neutral collision frequency is comparable to or larger than the ion gyrofrequency in the midlatitude E region ionosphere, the ions follow the neutrals in this region. Therefore, the Ca^+ acts as a tracer of the neutral atmosphere, and the observed K-H billow-like structure suggests that there was a strong vertical shear in the horizontal neutral wind. This is consistent with the wind shear theory of the E_s layer that ions become concentrated into thin layers by a vertical shear of the neutral wind (e.g., Mathews, 1998; Whitehead, 1989, and references therein). According to Larsen (2000), a K-H billow is embedded in the mean flow within the shear region and moves with it, and its horizontal scale is approximately 8 times as large as the vertical scale of the shear. As the observed vertical extent of the K-H billow-like structure was approximately 2 km, the horizontal wavelength was expected to be 16

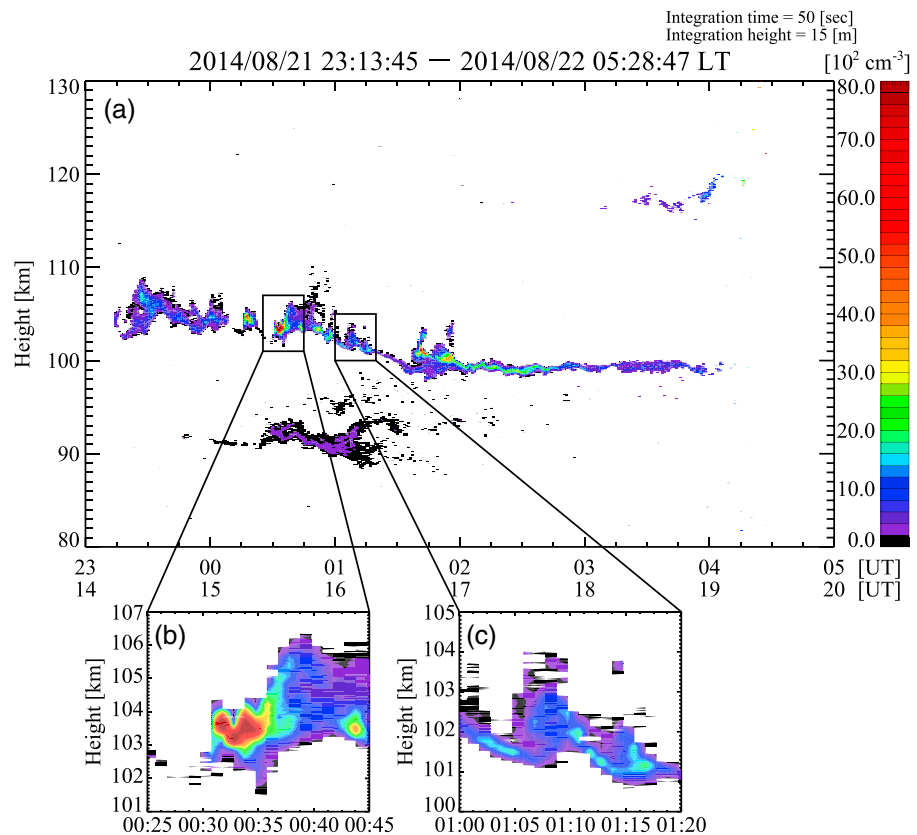


Figure 1. (a) Height-time-density plot of Ca^+ observed with a frequency-tunable resonance scattering lidar at National Institute of Polar Research in Japan. High (low) densities are shown by warm (cold) color. The local time is UTC + 9 hr. (b) A clump with high density is enlarged and displayed in the height range of 101–107 km and time range of 00:25–00:45 LT. (c) A Kelvin-Helmholtz billow-like structure is enlarged and displayed in the height range of 100–105 km and time range of 01:00–01:20 LT.

km. Since the observed duration of the K-H billow-like structure was 6–7 min, the background wind speed was estimated as ~ 40 m/s perpendicular to the billow axis. Another region of larger density irregularities (not enlarged) can be seen clearly between 01:30 and 02:00 LT.

Figure 2a shows the height of the maximum Ca^+ density in the main Ca^+_s layer as a function of time. The main layer descended with a speed of ~ 2.8 km/hr, from 107 km at 23:30 LT to ~ 100 km at 02:00 LT and stopped at a fixed height of ~ 100 km from 02:00 LT to 04:00 LT. After 04:00 LT, the data became noisy because of twilight contamination. This descending motion of the Ca^+_s layer is similar to a typical descent of the E_s layer observed with IS radars and ionosondes at night in the midlatitude ionosphere (e.g., Haldoupis, 2012; Mathews & Bekeny, 1979). According to the physical interpretation summarized in a review paper by Haldoupis (2012), vertical plasma convergence times are longer at lower altitudes, below 120 km, because of the ion-neutral collision. Therefore, E_s layer formation and descent between 110 and 90 km are controlled by the diurnal tide that phase-propagates downward (~ 1.0 km/hr) slower than semi-diurnal tides. On the other hand, our observation showed that the descending speed of the Ca^+_s layer was 2.8 km/hr between 107 and 100 km. This speed is close to the downward phase speed of semidiurnal tide rather than diurnal tide. The atmospheric waves with the wind shear cannot be determined without background wind measurements, but the height that the Ca^+_s layer stops descending, at ~ 100 km in this case, is probably determined by the balance between the forcing of the vertical wind shear gradient and the drag on vertical descent, which depends on the ratio of the ion-neutral collision frequency to the ion gyrofrequency ρ_i . If the vertical moving of the Ca^+ is solely caused by the zonal neutral wind without the polarization field, the vertical velocity (\bar{v}) of the Ca^+ during the descending phase can be expressed by the following equation (Cosgrove & Tsunoda, 2002)

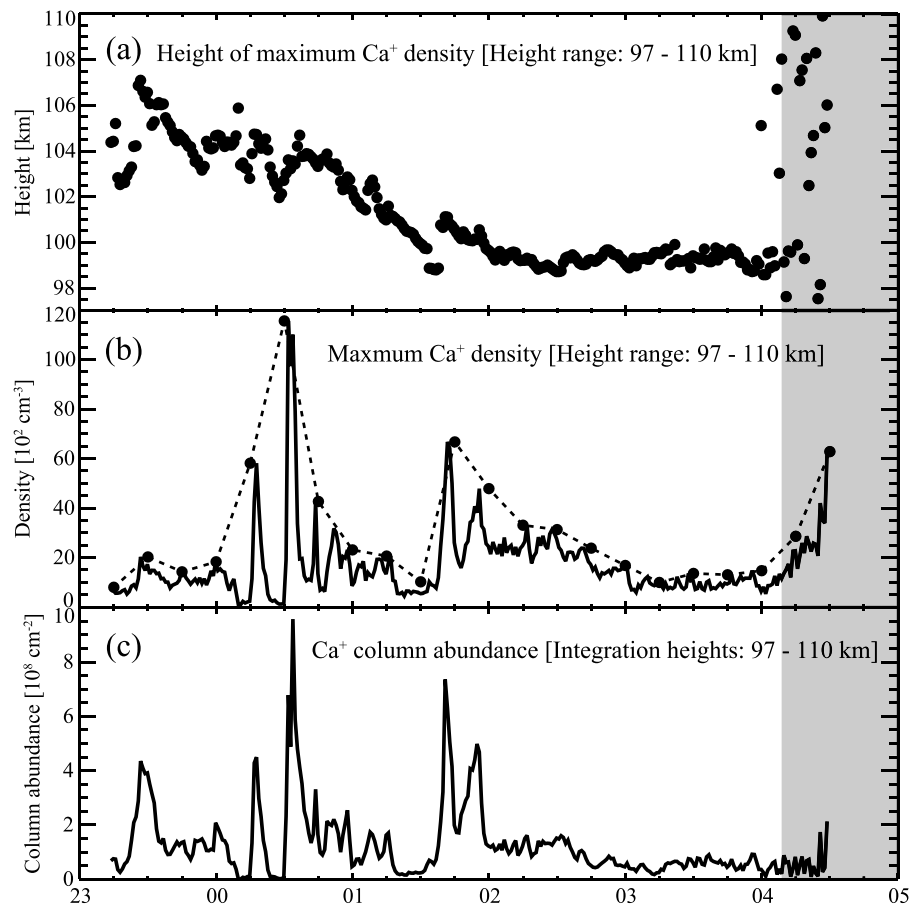


Figure 2. Time series of (a) height of the maximum Ca^+ density, (b) maximum Ca^+ density, and (c) Ca^+ column abundance between 97 and 110 km. The shadowed area refers to observations after the local sunrise (04:08 LT at an altitude of 100 km). In (b), the dots connected by a dashed line represent the maximum Ca^+ density in the 10-min window every 15 min. The Ca^+ densities in (b) and (c) are Ca^+ number density and column abundance deduced from background-subtracted photocounts subject to the criterion of minimal signal-to-noise ratio of 2.0.

$$\vec{v} = \frac{\rho_i}{1 + \rho_i} \cdot (\vec{u} \times \hat{b}) \cdot \cos I \quad (1)$$

where \hat{b} is the unit vector in the magnetic north direction, \vec{u} the zonal neutral wind velocity, and I the local geomagnetic inclination angle. According to the twelfth-generation International Geomagnetic Reference Field (IGRF-12) model (Thébault et al., 2015), I is 49.5° at Tachikawa (geomagnetic latitude/longitude: $27.1^\circ\text{N}/151.1^\circ\text{W}$). Using the ion-neutral collision frequency (Banks & Kockarts, 1973; Voiculescu & Ignat, 2003) for the densities of the nitrogen and oxygen molecules and the oxygen atoms, calculated by NRLMSISE-00 (Picone et al., 2002), ρ_i is 34.2 at an altitude of 100 km over Tachikawa. For the Ca^+ to follow the descending wind shear with a speed of 2.8 km/hr ($=0.78$ m/s), according to equation (1), a westward wind velocity of 41 m/s is required at 100 km. This speed is consistent with the background wind speed (~ 40 m/s) estimated from the duration of the K-H billow-like structure, assuming the dominance of the zonal neutral wind. At the lower altitude ρ_i is larger and the required balancing westward wind velocity would be faster; that is, the westward wind velocity is 51 m/s at an altitude of 99 km and 62 m/s at an altitude of 98 km. In other words, a westward wind velocity of ~ 40 m/s is too slow to maintain the downward descent of the Ca^+ layer at lower altitudes. As a result, the descent of the Ca^+ layer slowed down quickly and stopped at an altitude of ~ 100 km, as the atmospheric wave and wind shear passed through the layer there.

The temporal variation of the maximum Ca^+ density in the main layer between 97 and 110 km is shown in Figure 2b. The maximum density of the Ca^+ layer drastically changed between 5×10^2 and $145 \times 10^2 \text{ cm}^{-3}$ from 00:10 to 00:45 LT and from 01:30 to 02:00 LT to a lesser extent. After 02:00 LT, it decreased gradually.

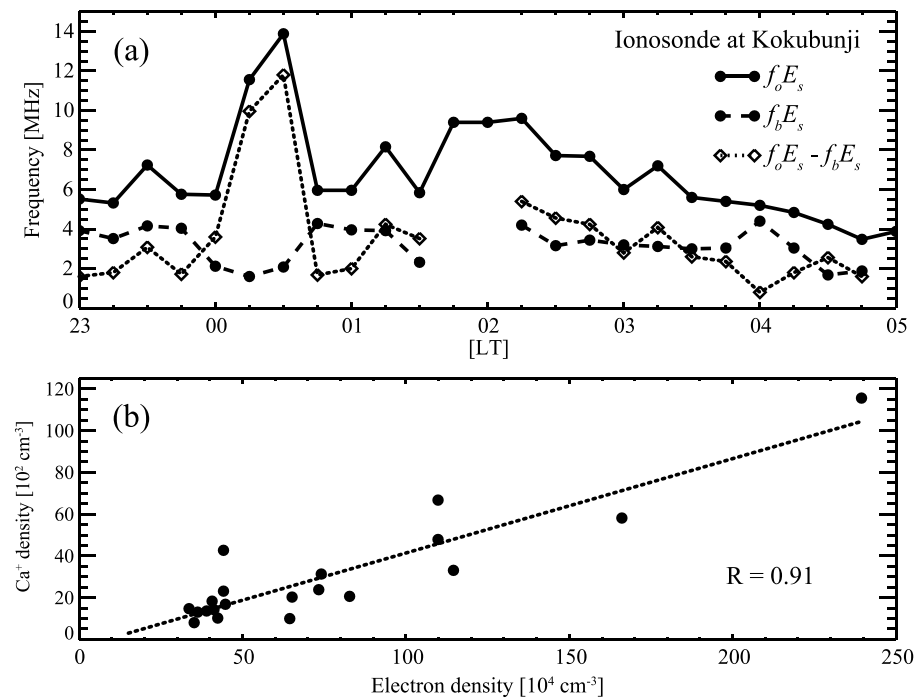


Figure 3. (a) The temporal variations of E_s layer parameters, f_oE_s (dots and solid line), f_bE_s (dots and dashed line), and $f_oE_s - f_bE_s (= \Delta f, \text{diamonds and dotted line})$, observed at Kokubunji during the night of 21 August 2014. (b) A correlation diagram between the maximum Ca^+ densities and maximum electron densities derived from f_oE_s . R is the correlation coefficient between them.

The temporal variation of the Ca^+ column abundance between 97 and 110 km is shown in Figure 2c. Here, the Ca^+ densities in Figures 2b and 2c are Ca^+ number density and column abundance deduced from background subtracted photocuts. They are calculated by subtracting the average background (noise) count from the raw signal profile. The average background count is the average count between 200 and 230 km where the Ca^+ density is supposed to be less than the minimum limit of detection of our lidar measurements. The Ca^+ column abundance indicated large variations with magnitudes of $5\text{--}11.5 \times 10^{12} \text{ m}^{-2}$ from 23:10 to 23:40 LT, from 00:10 to 00:45 LT, and from 01:30 to 02:00 LT. The large changes of the maximum density and the column abundance were observed only during the descending phase of the main Ca^+_s layer before 02:00 LT and were related to the irregular structures in the layer as seen in Figure 1a. During the stagnant period of the Ca^+_s layer at ~ 100 km after 02:00 LT, their variations were more than an order of magnitude smaller than before. The irregular structures in the descending phase of the main Ca^+_s layer were probably generated by disturbances associated with a strong vertical shear in the horizontal neutral wind and the E - F coupling instability. The main Ca^+_s layer stayed at ~ 100 -km altitude apart from the descending wind shear, no more disturbed by the wind shears, and it had no irregular structure.

3.2. E_s Layer

The temporal variations of the E_s layer parameters, f_oE_s and f_bE_s , observed at Kokubunji during the night of 21 August 2014 are shown in Figure 3a by dots connected with a solid line and a dashed line, respectively. The f_oE_s varied between 5 and 14 MHz throughout the night. The frequency differences, $\Delta f = f_oE_s - f_bE_s$, exceeding 1 MHz were observed for most of the night except from 01:45 LT to 02:00 LT. The results show that the E_s layer was spatially inhomogeneous, and the maximum electron density in the E_s layer changed drastically with time. Large values of f_oE_s appeared between 00:15 LT and 00:30 LT and between 01:45 LT and 02:15 LT. At the same period, the maximum Ca^+ densities in the Ca^+_s layer were enhanced, as shown in Figure 2b. The black dots connected by a dotted line in Figure 2b indicate the maximum Ca^+ densities in 10-min windows every 15 min. Figure 3b shows a correlation diagram between the maximum Ca^+ densities

and the maximum electron densities estimated from f_oE_s . It shows a strong positive correlation, with a correlation coefficient (R) of 0.91. This result is consistent with a good correlation between the Ca^+ density and the electron density, respectively, observed by the lidar and the IS radar at Arecibo Observatory (Raizada et al., 2012). The spatial inhomogeneity of the E_s layer and the variable maximum electron density in the E_s layer were probably caused by the irregular structures of 6- to 7-min duration observed in the Ca^+ layer. The ratio of the maximum Ca^+ density to the maximum electron density in Figure 3b is $\sim 0.45\%$, a value consistent with that of 0.3–0.5% observed at Arecibo Observatory at 101–105 km (Raizada et al., 2012).

3.3. Relationship Between the MSTIDs and the Irregular Structures in the Ca^+ Layer

On 21–22 August 2014, MSTIDs were observed by a GNSS receiver array, from $\sim 21:00$ LT. The GPS TEC maps over Japan at 00:32 LT and 02:35 LT are shown in the left panels of Figure 4. The GPS TEC map at 00:32 LT (top left panel) shows the wave-fronts of the MSTID stretched from the NNW to the SSE with a typical horizontal wavelength of ~ 230 km. The MSTID propagated southwestward with a horizontal phase speed and a period of ~ 50 m/s and ~ 75 min, respectively. The horizontal phase speed was getting slower after 02:00 LT, and then the wave-fronts were broken gradually and became patchy structures around 02:35 LT as shown in the bottom panels of Figure 4. The right panels of Figure 4 are detailed maps of the region around the NIPR in Tachikawa (34.7°N , 139.4°E); the geographic location is indicated by the white dot inside the black circle. The declination and inclination of the geomagnetic field at an altitude of 100 km over the NIPR, calculated by the IGRF-12 model, are -6.9° and 49.5° , respectively. The black dot inside the white circle at 34.2°N , 139.6°E in the figure indicates the location (hereinafter referred to as F -NIPR) where the geomagnetic field line through its ionospheric F region at 300 km intersects the Ca^+ layer at 100 km over the NIPR; that is, the white dot and the black dot are on a common magnetic flux tube. The temporal variations in GPS TECs at the F -NIPR and the NIPR from 23:00 LT to 04:00 LT are plotted in Figure 5a by black and gray lines, respectively. The amplitudes of the GPS TEC variations at the F -NIPR and NIPR were similar in magnitude, $1\text{--}2 \times 10^{16} \text{ m}^{-2}$, before 02:00 LT, but the phases were different, especially at 01:00–02:00 LT the variation at the F -NIPR was delayed by nearly 90° relative to that at the NIPR. Notice that the GPS TEC variations at the F -NIPR were positive at 23:10–23:30 LT, 00:00–00:40 LT, and 01:30–02:00 LT.

The temporal variation of the Ca^+ column abundance between 80 and 130 km is shown in Figure 5b. Drastic enhancements of the Ca^+ column abundance can be seen around 23:25 LT, 00:15 LT, 00:30 LT, 01:40 LT, and 01:55 LT. Interestingly, these enhancements were coincident with positive variations in the GPS TEC variations at the F -NIPR (not at the NIPR), although the durations of the Ca^+ column abundance enhancements were shorter than those of the positive GPS TEC variations. The GPS TEC variations contain electron column abundance variations not only in the F region but also in the E region. Since the ratio of the maximum Ca^+ density to the maximum electron density as shown in Figure 3b is $\sim 0.45\%$ the largest observed Ca^+ column abundance which was $10.1 \times 10^{12} \text{ m}^{-2}$ around 00:30 LT corresponds to an estimated E region electron column abundance of $\sim 2.2 \times 10^{15} \text{ m}^{-2}$ as shown in Figure 5b. Further, since the (peak-to-peak) GPS TEC variation as noted in Figure 5a was $\sim 4 \times 10^{16} \text{ m}^{-2}$, the electron column abundance in the E region was less than 6% of the GPS TEC variation of the MSTIDs. Therefore, the contributions of the E region including the E_s layers to the GPS TEC variations were negligible, and the GPS TEC variations associated with the MSTIDs represented mainly the electron column abundance variations in the F region. The enhancement of the Ca^+ column abundance was coincident with the positive GPS TEC variations at the F -NIPR rather than the NIPR (Figures 5a and 5b). The observations support the theory with regard to the phase relationship between the MSTIDs and E_s , suggesting that the MSTIDs and the plasma density irregularities of the E_s layer were electrically coupled through the geomagnetic field line as predicted by the F - F coupling instability theory (Cosgrove & Tsunoda, 2002, 2004; Yokoyama et al., 2009). Such direct coupling between the plasma density irregularities of the E_s layer and the MSTIDs in the F region could not be revealed by the E region and F region observations from a single site (Hysell et al., 2016).

As discussed, the GPS TEC variations associated with the MSTIDs were large before 02:00 LT when the Ca^+ column abundance was enhanced repeatedly with surges in the descending phase of the main Ca^+ layer. In contrast, the amplitude of the GPS TEC variation at the F -NIPR decreased by an order of magnitude or more after 02:00 LT when the Ca^+ column abundance showed no significant enhancements during the stagnant period of the main Ca^+ layer at ~ 100 km. The disappearance of the GPS TEC variation is also

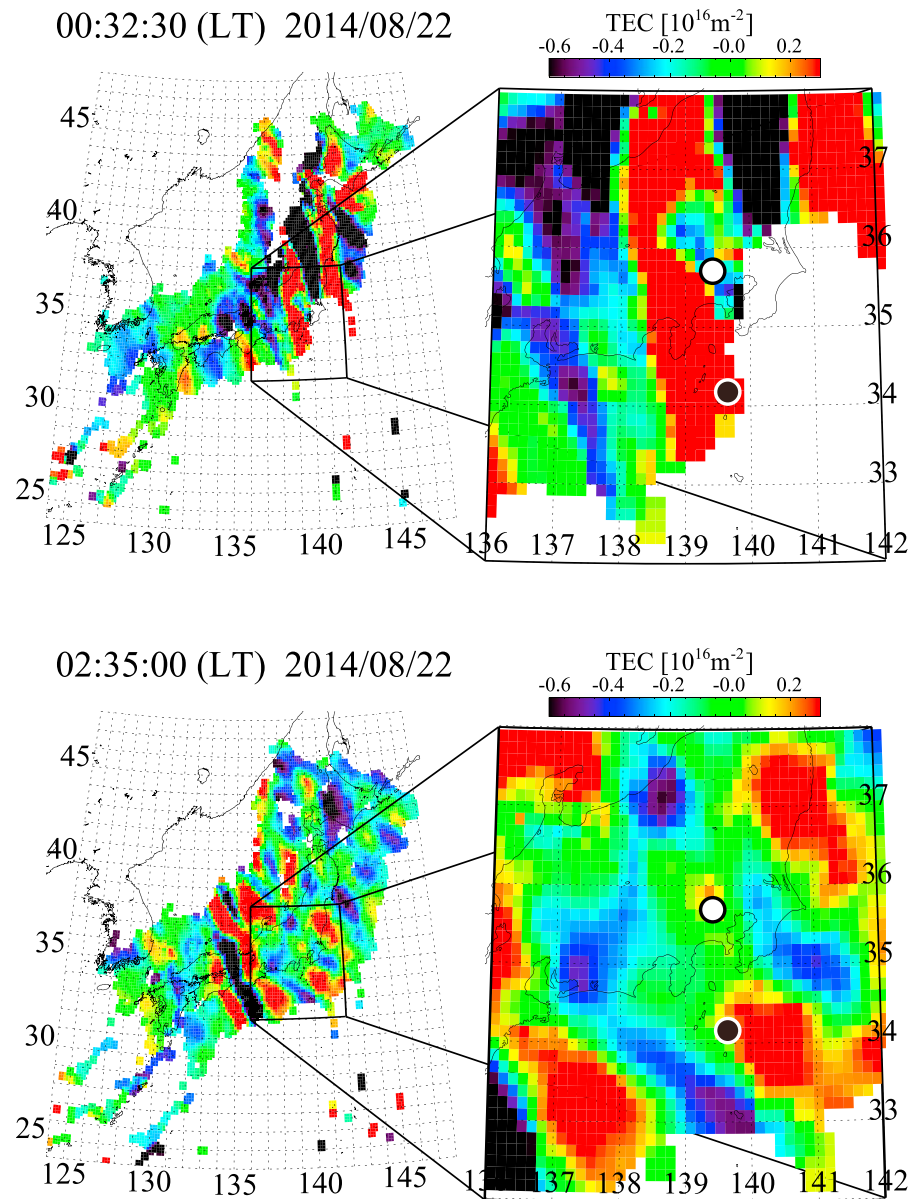


Figure 4. The GPS TEC maps over Japan obtained at 00:32:30 LT and 02:35:00 LT on 22 August 2014 are displayed in the left panels. The right panels show enlarged maps of the region around the NIPR in Tachikawa (indicated by the white dot inside the black circle). The black dot inside the white circle represents the location (F -NIPR) at an altitude of 300 km, geomagnetically connected to the Ca^+ layer at 100 km over the NIPR. TEC = total electron content; NIPR = National Institute of Polar Research.

the result of the E - F coupling in that the MSTID structure cannot be sustained without the density irregularities in the E_s layer. This observational result is consistent with the three-dimensional numerical model studies of Yokoyama et al. (2009), whose simulation showed that the perturbation in the F region is quickly suppressed without perturbations in the E_s layer because polarization in the F region is shorted out by the uniform E_s layer. The drastic enhancements in the Ca^+ column abundance could be also a result of the E - F coupling process that reinforced the disturbances caused by the neutral wind shear (Yokoyama et al., 2009).

Another long night Ca^+_s layer observation occurred on 24 December 2014 between 20 and 07 LT (see Figure 1 in Ejiri et al., 2019). Similar to the 21 August 2014 observation, the Ca^+_s layer descended before 02:00 LT

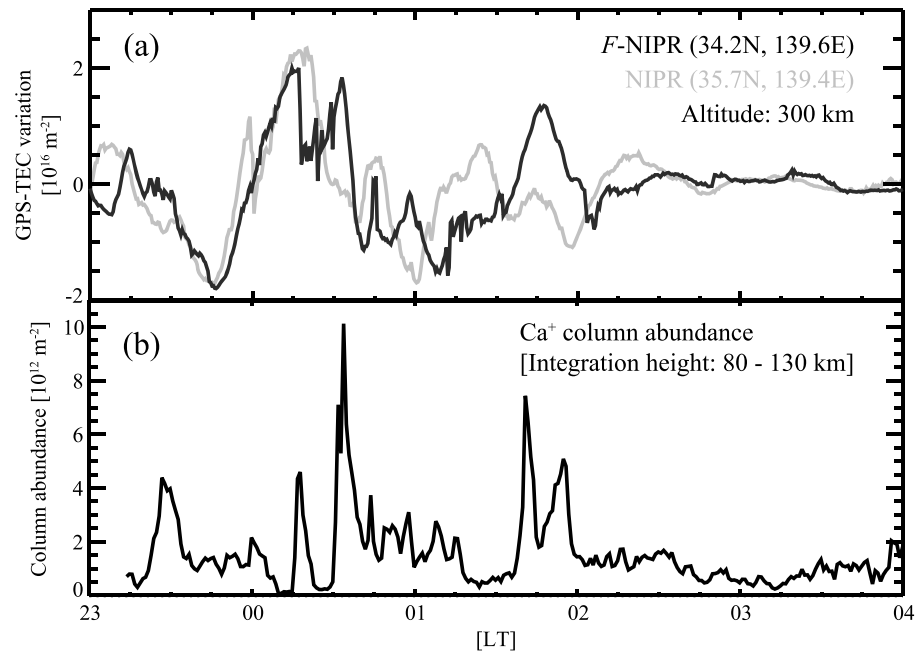


Figure 5. Temporal variations in (a) the GPS TECs and (b) the Ca^+ column abundance from 23:00 LT to 04:00 LT. In panel (a), black and gray lines indicate the GPS TEC variations at the *F*-NIPR and over the NIPR, respectively. TEC = total electron content; NIPR = National Institute of Polar Research.

and stopped at around 100-km altitude afterward. Although several instability structures were seen in the Ca^+ layer, the big surges in Ca^+ column abundance as shown in Figure 6b were absent, contrary to that on 21 August 2014 (see Figure 5b). Correspondingly, the MSTIDs were not seen in the GPS TEC variation on 24 December 2014 as displayed in Figure 6a. That the MSTIDs did not appear when there were no big

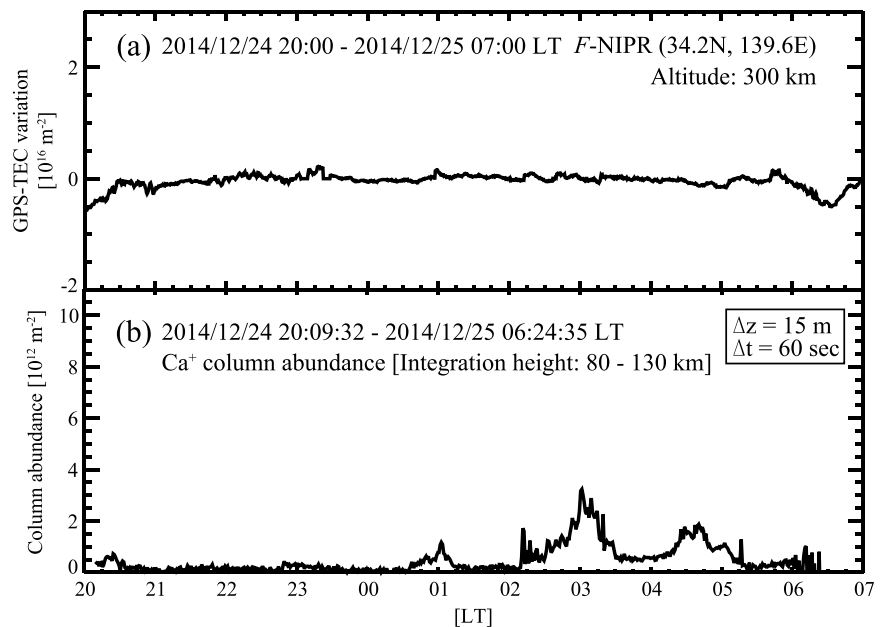


Figure 6. Temporal variations in (a) the GPS TECs and (b) the Ca^+ column abundance from 20:00 LT on 24 December to 07:00 LT on 25 December 2014. Neither big surges in Ca^+ column abundance nor medium-scale traveling ionospheric disturbances were seen throughout the night. The Ca^+ densities are the same data as used in Ejiri et al. (2019) but integrated for 1 min (5-s resolution originally). TEC = total electron content; NIPR = National Institute of Polar Research.

E_s density irregularities, even if the E_s layer was generated in the E region, also suggests a strong relationship between the E_s density irregularities and the MSTIDs.

4. Summary

The density irregularities of the E_s layer and the MSTIDs in the ionospheric F region were observed simultaneously with a frequency-tunable resonance scattering lidar, an ionosonde, and a GNSS receiver array in the nighttime midlatitude ionosphere on 21–22 August 2014. The maximum densities of Ca^+ observed by the lidar at the NIPR in Tachikawa and the maximum densities of electrons in the E_s layer obtained by the ionosonde at the NICT in Kokubunji had a strong positive correlation, with a correlation coefficient of 0.91, suggesting the variation of the Ca^+ density profiles represents the fine structures of plasma irregularities in the E_s layer. The Ca^+ layer corresponding to the E_s layer descended with a speed of ~ 2.8 km/hr before it stopped at ~ 100 km around 02:00 LT. During the descent, the Ca^+ layer showed repeated surges of disturbed structures including K-H billow-like structures with the intense change of the Ca^+ column abundance, presumably in response to the vertical shear in the neutral horizontal wind and the E - F coupling instability. The descent of the Ca^+ layer stopped at $\sim 02:00$ LT and settled there at an altitude of ~ 100 km without large variations in the Ca^+ column abundance until sunrise. The reason that the Ca^+ layer stops descending at ~ 100 km is that the $\vec{u} \times \hat{b}$ forcing is now too small to overcome the increasing ion drag, that is, larger ratio of the ion-neutral collision frequency to the ion gyrofrequency at lower altitudes. As a result, the descent of the Ca^+ layer stopped at an altitude of ~ 100 km, while the wind shear continued to descend.

The temporal variation of the Ca^+ column abundance around the altitude of 100 km over the NIPR was found to be in synchronization with the GPS TEC variation associated with the MSTIDs at an altitude of 300 km over the F -NIPR located on a common magnetic flux tube with the Ca^+ layer at 100 km over the NIPR. This situation agrees with the E - F coupling instability predicted by three-dimensional numerical models. Both the Ca^+ column abundance enhancements and the large GPS TEC variation were seen only in the descending phase of the main Ca^+ layer, and they disappeared when the descent of the Ca^+ layer stops. Therefore, the atmospheric wave, such as semidiurnal tide and diurnal tide, in the E region that induces the descent of the Ca^+ layer is essential for the growth of the E - F coupling instability. Our simultaneous observation with the Ca^+ resonance scattering lidar, ionosonde, and GEONET clearly revealed the predicted coupling features between the E_s layer and the F region ionosphere. Simultaneous observation with the thermospheric neutral wind and the electric field will be required to further understand the details of the E - F coupling process.

Acknowledgments

This work was supported by the JSPS Grant-in-Aid for challenging Exploratory Research (grant 15K13575) and the Project Research KP-2 Project of the National Institute of Polar Research. The lidar data can be accessed at the website (<http://id.nii.ac.jp/1291/00014958/>). GEONET GPS data were provided by the Geographical Survey Institute of Japan. Ionosonde data at Kokubunji were provided by the World Data Center for Ionosphere through the National Institute of Information and Communications Technology, Tokyo. The production of this paper was supported by an NIPR production subsidy.

References

- Banks, P. M., & Kockarts, G. (1973). *Aeronomy, Part A* (pp. 184–239). New York, NY: Academic Press.
- Chu, X., & Papen, G. C. (2005). Resonance fluorescence lidar for measurements of the middle and upper atmosphere. In T. Fujii, & T. Fukuchi (Eds.), *The Book of Laser Remote Sensing* (pp. 179–432). Boca Raton, Fla: CRC Press, Taylor and Francis Group. <https://doi.org/10.1201/9781420030754.ch5>
- Cosgrove, R. B., & Tsunoda, R. T. (2002). A direction-dependent instability of sporadic- E layers in the nighttime midlatitude ionosphere. *Geophysical Research Letters*, 29(18), 1864. <https://doi.org/10.1029/2002GL014669>
- Cosgrove, R. B., & Tsunoda, R. T. (2004). Instability of the $E - F$ coupled nighttime midlatitude ionosphere. *Journal of Geophysical Research*, 109, A04305. <https://doi.org/10.1029/2003JA010243>
- Ejiri, M. K., Nakamura, T., Tsuda, T. T., Nishiyama, T., Abo, M., Takahashi, T., et al. (2019). Vertical fine structure and time evolution of plasma irregularities in the E_s layer observed by a high-resolution Ca^+ lidar. *Earth, Planets and Space*, 71(1), 3. <https://doi.org/10.1186/s40623-019-0984-z>
- Gerding, M., Alpers, M., Höffner, J., & von Zahn, U. (2001). Sporadic Ca and Ca^+ layers at mid-latitudes: Simultaneous observations and implications for their formation. *Annales de Geophysique*, 19(1), 47–58. <https://doi.org/10.5194/angeo-19-47-2001>
- Gerding, M., Alpers, M., von Zahn, U., Rollason, R. J., & Plane, J. M. C. (2000). The atmospheric Ca and Ca^+ layers: Midlatitude observations and modeling. *Journal of Geophysical Research*, 105, 27,131–27,146. <https://doi.org/10.1029/2000JA900088>
- Granier, G., Jégou, J. P., & Mégie, G. (1985). Resonant lidar detection of Ca and Ca^+ in the upper atmosphere. *Geophysical Research Letters*, 12(10), 655–658. <https://doi.org/10.1029/GL012i010p00655>
- Haldoupis, C. (2012). Midlatitude sporadic-E. A typical paradigm of atmosphere-ionosphere coupling. *Space Science Reviews*, 168(1–4), 441–461. <https://doi.org/10.1007/s11214-011-9786-8>
- Hysell, D., Larsen, M., Fritts, D., Laughman, B., & Sulzer, M. (2018). Major upwelling and overturning in the mid-latitude F region ionosphere. *Nature Communications*, 9(1), 3326. <https://doi.org/10.1038/s41467-018-05809-x>
- Hysell, D., Larsen, M., & Sulzer, M. (2016). Observational evidence for new instabilities in the mid-latitude E and F region. *Annales de Geophysique*, 34(11), 927–941. <https://doi.org/10.5194/angeo-34-927-2016>
- Istomin, V. G. (1963). Ions of extra-terrestrial origin in the Earth ionosphere. *Planetary and Space Science*, 11(2), 173–174. [https://doi.org/10.1016/0032-0633\(63\)90140-5](https://doi.org/10.1016/0032-0633(63)90140-5)

- Kurihara, J., Koizumi-Kurihara, Y., Iwagami, N., Suzuki, T., Kumamoto, A., Ono, T., et al. (2010). Horizontal structure of sporadic *E* layer observed with a rocket-borne magnesium ion imager. *Journal of Geophysical Research*, *115*, A12318. <https://doi.org/10.1029/2009JA014926>
- Larsen, M. F. (2000). A shear instability seeding mechanism for quasiperiodic radar echoes. *Journal of Geophysical Research*, *105*(A11), 24,931–24,940. <https://doi.org/10.1029/1999JA000290>
- Mathews, J. D. (1998). Sporadic *E*: Current views and recent progress. *Journal of Atmospheric and Solar - Terrestrial Physics*, *60*(4), 413–435. [https://doi.org/10.1016/S1364-6826\(97\)00043-6](https://doi.org/10.1016/S1364-6826(97)00043-6)
- Mathews, J. D., & Bekeny, F. S. (1979). Upper atmospheric tides and the vertical motion of ionospheric sporadic layers at Arecibo. *Journal of Geophysical Research*, *84*(A6), 2743–2750. <https://doi.org/10.1029/JA084iA06p02743>
- Miller, C. A., Swartz, W. E., Kelley, M. C., Mendillo, M., Nottingham, D., Scali, J., & Reinisch, B. (1997). Electrodynamics of midlatitude spread *F*: 1. Observations of unstable, gravity wave-induced ionospheric electric fields at tropical latitudes. *Journal of Geophysical Research*, *102*(A6), 11,521–11,532. <https://doi.org/10.1029/96JA03839>
- Ogawa, T., Takahashi, O., Otsuka, Y., Nozaki, K., Yamamoto, M., & Kita, K. (2002). Simultaneous middle and upper atmosphere radar and ionospheric sounder observations of midlatitude *E* region irregularities and sporadic *E* layer. *Journal of Geophysical Research*, *107*(A10), 1275. <https://doi.org/10.1029/2001JA900176>
- Otsuka, Y., Onoma, F., Shiokawa, K., Ogawa, T., Yamamoto, M., & Fukao, S. (2007). Simultaneous observations of nighttime medium-scale traveling ionospheric disturbances and *E* region field-aligned irregularities at midlatitude. *Journal of Geophysical Research*, *112*, A06317. <https://doi.org/10.1029/2005JA011548>
- Otsuka, Y., Tani, T., Tsugawa, T., & Ogawa, T. (2008). Statistical study of relationship between medium-scale traveling ionospheric disturbance and sporadic *E* layer activities in summer night over Japan. *Journal of Atmospheric and Solar - Terrestrial Physics*, *70*(17), 2196–2202. <https://doi.org/10.1016/j.jastp.2008.07.008>
- Perkins, F. (1973). Spread *F* and ionospheric currents. *Journal of Geophysical Research*, *78*(1), 218–226. <https://doi.org/10.1029/JA078i001p00218>
- Picone, J. M., Hedin, A. E., & Drob, D. P. (2002). NRLMSISE-00 empirical model of the atmosphere: Statistical comparisons and scientific issues. *Journal of Geophysical Research*, *107*(A12), 1468. <https://doi.org/10.1029/2002JA009430>
- Raizada, S., Tepley, C. A., Aponte, N., & Cabassa, E. (2011). Characteristics of neutral calcium and Ca^+ near the mesopause, and their relationship with sporadic ion/electron layers at Arecibo. *Geophysical Research Letters*, *38*, L09103. <https://doi.org/10.1029/2011GL047327>
- Raizada, S., Tepley, C. A., Williams, B. P., & García, R. (2012). Summer to winter variability in mesospheric calcium ion distribution and its dependence on sporadic *E* at Arecibo. *Journal of Geophysical Research*, *117*, A02303. <https://doi.org/10.1029/2011JA016953>
- Saito, A., Fukao, S., & Miyazaki, S. (1998). High resolution mapping of TEC perturbations with the GSI GPS Network over Japan. *Geophysical Research Letters*, *25*(16), 3079–3082. <https://doi.org/10.1029/98GL52361>
- Saito, A., Nishimura, M., Yamamoto, M., Fukao, S., Kubota, M., Shiokawa, K., et al. (2001). Traveling ionospheric disturbances detected in the FRONT campaign. *Geophysical Research Letters*, *28*(4), 689–692. <https://doi.org/10.1029/2000GL011884>
- Saito, S., Yamamoto, M., Hashiguchi, H., Maegawa, A., & Saito, A. (2007). Observational evidence of coupling between quasiperiodic echoes and medium scale traveling ionospheric disturbances. *Annales de Geophysique*, *25*(10), 2185–2194. <https://doi.org/10.5194/angeo-25-2185-2007>
- She, C.-Y. (2001). Spectral structure of laser light scattering revisited bandwidths of nonresonant scattering lidars. *Applied Optics*, *40*(27), 4875–4884. <https://doi.org/10.1364/AO.40.004875>
- Shiokawa, K., Ihara, C., Otsuka, Y., & Ogawa, T. (2003). Statistical study of nighttime medium-scale traveling ionospheric disturbances using midlatitude airglow images. *Journal of Geophysical Research*, *108*(A1), 1052. <https://doi.org/10.1029/2002JA009491>
- Swartz, W. E., Kelley, M. C., & Aponte, N. (2009). *E*- and *F*-region coupling between an intense sporadic *E* layer and a mesoscale traveling ionospheric disturbance. *Annales de Geophysique*, *27*(6), 2475–2482. <https://doi.org/10.5194/angeo-27-2475-2009>
- Tepley, C. A., Raizada, S., Zhou, Q., & Friedman, J. S. (2003). First simultaneous observations of Ca^+ , K, and electron density using lidar and incoherent scatter radar at Arecibo. *Geophysical Research Letters*, *30*(1), 1009. <https://doi.org/10.1029/2002GL015927>
- Thébault, E., Finlay, C. C., Beggan, C. D., Alken, P., Aubert, J., Barrois, O., et al. (2015). International Geomagnetic Reference Field: The 12th generation. *Earth, Planets and Space*, *67*(1), 1–19. <https://doi.org/10.1186/s40623-015-0228-9>
- Tsunoda, R. T. (2006). On the coupling of layer instabilities in the nighttime midlatitude ionosphere. *Journal of Geophysical Research*, *111*, A11304. <https://doi.org/10.1029/2006JA011630>
- Voiculescu, M., & Ignat, M. (2003). Vertical motion of ionization induced by the linear interaction of tides with planetary waves. *Annales de Geophysique*, *21*(7), 1521–1529. <https://doi.org/10.5194/angeo-21-1521-2003>
- Whitehead, J. D. (1961). The formation of sporadic-*E* layers in the temperate zones. *Journal of Atmospheric and Terrestrial Physics*, *20*, 49–58. [https://doi.org/10.1016/0021-9169\(61\)90097-6](https://doi.org/10.1016/0021-9169(61)90097-6)
- Whitehead, J. D. (1989). Recent work on mid-latitude and equatorial sporadic-*E*. *Journal of Atmospheric and Solar - Terrestrial Physics*, *51*(5), 401–424. [https://doi.org/10.1016/0021-9169\(89\)90122-0](https://doi.org/10.1016/0021-9169(89)90122-0)
- Yamamoto, M., Fukao, S., Ogawa, T., Tsuda, T., & Kato, S. (1992). A morphological study on midlatitude *E*-region field-aligned irregularities observed with the MU radar. *Journal of Atmospheric and Solar - Terrestrial Physics*, *54*(6), 769–777. [https://doi.org/10.1016/0021-9169\(92\)90115-2](https://doi.org/10.1016/0021-9169(92)90115-2)
- Yamamoto, M., Fukao, S., Woodman, R. F., Ogawa, T., Tsuda, T., & Kato, S. (1991). Mid-latitude *E*-region field-aligned irregularities observed with the MU radar. *Journal of Geophysical Research*, *96*, 15,943–15,949. <https://doi.org/10.1029/91JA01321>
- Yamamoto, M., Komoda, N., Fukao, S., Tsunoda, R. T., Ogawa, T., & Tsuda, T. (1994). Spatial structure of the *E*-region field-aligned irregularities revealed by the MU radar. *Radio Science*, *29*(1), 337–347. <https://doi.org/10.1029/93RS01846>
- Yokoyama, T., Hysell, D. L., Otsuka, Y., & Yamamoto, M. (2009). Three dimensional simulation of the coupled Perkins and E_s layer instabilities in the nighttime midlatitude ionosphere. *Journal of Geophysical Research*, *114*, A03308. <https://doi.org/10.1029/2008JA013789>
- Yokoyama, T., & Hysell, D. L. (2010). A new midlatitude ionosphere electrodynamics coupling model (MIECO): Latitudinal dependence and propagation of medium-scale traveling ionospheric disturbances. *Geophysical Research Letters*, *37*, L08105. <https://doi.org/10.1029/2010GL042598>
- Zhou, C., Tang, Q., Huang, F., Liu, Y., Gu, X., Lei, J., et al. (2018). The simultaneous observations of nighttime ionospheric *E* region irregularities and *F* region mediumscale traveling ionospheric disturbances in midlatitude China. *Journal of Geophysical Research: Space Physics*, *123*, 5195–5209. <https://doi.org/10.1029/2018JA025352>